AN UNUSUAL METAL TEMPLATING EFFECT SWITCHING AN N_2S_2 LIGAND TO A BINUCLEATING, TRIDENTATE S_2O_2 LIGAND

An Undergraduate Research Scholars Thesis

by

HAO ANH NGUYEN

Submitted to the Undergraduate Research Scholars program at
Texas A&M University
in partial fulfillment of the requirements for the designation as an

UNDERGRADUATE RESEARCH SCHOLAR

Approved by Research Advisor: Dr. Marcetta Y. Darensbourg

May 2020

Major: Chemistry

TABLE OF CONTENTS

ABSTRACT

An Unusual Metal Templating Effect Switching An N_2S_2 Ligand To A Binucleating, Tridentate S_2O_2 Ligand

Hao A. Nguyen
Department of Chemistry
Texas A&M University

Research Advisor: Dr. Marcetta Y. Darensbourg
Department of Chemistry
Texas A&M University

Natural metalloenzymes not only display extraordinary catalytic activities in biological systems, but also are models for chemists to design organometallic catalysts. Bioinorganic chemical researchers in this field focus on the metal-containing active sites of enzymes. Interestingly, the selections of metal and the responses to the metal substitution of these enzymes are usually surprising due to the unpredictability and variety.

A tripeptide Cys-Gly-Cys biomimetic N_2S_2 ligand class, which is found in acetyl-CoA-synthase active site, has caught attention due to its capability of encapsulating a metal cation giving rise to a variety of MN_2S_2 units. It has been shown that these units can trap extraneous metal ions using the additional lone pairs of the thiolate sulfurs while keeping the MN_2S_2 unit intact. Here, when choosing M-*ema* as the MN_2S_2 ligand to react with $Mn(CO)_5Br$ (*ema* = N,N'- ethylenebis(2-mercaptoacetamide)), an unprecedented result was obtained, in which M is removed from the tetradentate tight binding site and *ema* becomes a tridentate binucleating S_2O_2 ligand to a two-manganese bimetallic system. Characterizations of this novel compound $[Mn(CO)_3]_2(H_2ema)$ were achieved by using infrared spectroscopy, X-Ray diffraction, nuclear magnetic resonance spectroscopy, and mass spectrometry.

Different synthetic approaches to $[Mn(CO)_3]_2(H_2ema)$ with modified starting materials reveal a fascinating metal-templated process where folding the backbone of *ema* ligand is essential to target the final product. This folding process is also reminiscent of tight loops in proteins. The solid-state structure of $[Mn(CO)_3]_2(H_2ema)$ determined via X-ray diffraction shows a pseudo-octahedral geometry around each manganese center which has two bridging thiolate sulfurs, three carbonyls, and one carboxamide oxygen. In addition, two five-membered Mn-S-CH_2-C-O rings in which manganese centers reside both hard and soft ligand donor sites suggest prospective applications and exciting reactivities of this complex.

Reactivity studies for $[Mn(CO)_3]_2(H_2ema)$ were also conducted. $^{13}CO/^{12}CO$ exchange experiments in different solvents showed that chemical environments of the three CO ligands are not equivalent. Deprotonation reaction of $[Mn(CO)_3]_2(H_2ema)$ was successful suggesting that the compound may be catalytic active.

Moreover, Re and Fe analogues of $[Mn(CO)_3]_2(H_2ema)$ have also been of our interest because of the recent and unique applications of Re and Fe complexes. While many compounds of Re have been extensively used in radiopharmaceuticals, the replacement of Mn centers by Fe would advance our exploration in study of bio-inspired organometallic complexes because Fe ersatz small-molecule mimics have been heavily studied in the last two decades and shown evidence of regioselectivity in ligand substitution. Although $[Re(CO)_3]_2(H_2ema)$ has been successfully prepared and shown similar properties to its analogous Mn compound, the synthesis of $[Fe(CO)_3]_2(H_2ema)$ has faced a challenge because of the instability of the starting material. Lastly, the structures of two related complexes, the Mn_4S_4 cluster and the $[Mn(CO)_3]_2$(*half-ema*), are also reported.

DEDICATION

I dedicate my dissertation work to my family with a huge feeling of gratitude to my loving parents, my brother Danh and his wife, as well as my sister Anh have never left my side and are very special. This work is also dedicated to all my professors and mentors for nurturing my childish curiosity and ambitions. I started my education career with zero idea how I would become a scientist, but with the words of wisdom from my professors and mentors I am now confident in being the person I want to be. To Dr. Brian Dolinar, who was there on my very first days of research, and my mentor Trung Le, who was with me side by side in this project, this dissertation represents my admiration and respect for you. To my research advisors Dr. Marcetta Darensourg and Dr. Kim Dunbar, I always feel lucky and honored to have an opportunity to work for the greatest women in the chemical society. Especially to Dr. Darensbourg, your brilliant guidance and invaluable advice are crucial to my success in undergraduate study. To all of my other teachers, mentors, teaching assistants, and advisors including Alyssia Lambert, Alison Walker Stromdahl, Laurie Miller, Dr. Holly Gaede, Dr. Tamara Powers Pierce Pham, Hieu Nguyen, Ellen Song, Freddy Ortiz, and hundreds of other wonderful people.

To my friends, as I promised to include your names in my Nobel prize acceptance speech if I ever get one, I want to have your names here as a significant part of my career: Mona Fattahi, Eric Shrader, Rachel Watts, Megan Welch, Kyle Bordovsky, Eliza Piccirillo, and Kristen Akin. Also, to other amazing friends: Karan Hooda, Danielle Burget, Ela Mo, Haley Naumann, Yunuen Avila-Martinez, Qui To, Anh Phan, Anh Le, My Nguyen, Khoa Nguyen, Richard Denton, and CheungHing Lam. And to all my friends at Texas A&M University and Pierce College, without you, I would not be able to finish this work. Thank you.

ACKNOWLEDGMENTS

I would like to thank my research advisors Dr. Marcetta Darensbourg and Dr. Kim Dunbar and my mentors Dr. Brian Dolinar and Mr. Trung Le for their guidance and support throughout my time at Texas A&M.

Thanks also go to my friends and colleagues and the department faculty and staff for making my time at Texas A&M University a great experience.

Finally, thanks to my mother and father for their encouragement and to my brother, sister, and friends.

NOMENCLATURE

DCM	Dichloromethane
ESI-MS	Electrospray ionization mass spectrometry
FT-IR	Fourier-transform infrared spectroscopy
NMR	Nuclear magnetic resonance
THF	Tetrahydrofuran

CHAPTER I

INTRODUCTION

Nature provides a number of metalloenzymes whose outstanding catalytic activity in biological systems has not been fully understood. Designing small molecules that have similar features as natural enzymes is an important approach that chemists has progressed in order to explore new useful catalysts. The Cys−X−Cys tripeptide motifs, which can be found in active sites of Acetyl-CoA synthase, nitrile hydratase, and thiocyanate hydratase are great platforms for the syntheses of biomimetic molecules (Figure 1).[1-4] These motifs offer the contiguous, tetradentate N_2S_2 metal-binding sites that have been extensively studied. [5]

MN_2S_2 as metalloligands to transition metals

Research in the past decades has successfully synthesized plenty of coordination complexes of transition metals with the tetradentate $[N_2S_2]^{2-}$ ligation (Figure 2).[5-8] If the transition metal is nickel, iron, or cobalt, the compounds are respectively related to the acetyl-CoA synthase, nitrile hydratase, and thiocyanate hydratase active site structures. The positions and distances of the N–S and N–N around a metal center are appropriate for creating a cis-orientation thiolate terminal to trap an exogeneous metal.[4] In other words, the MN_2S_2 can act as a class of metalloligands, in which, the cis-dithiolates site provides lone pairs that can serve as a bidentate S-donor ligand to a metal ion (Figure 2C).[8,9] In some cases, monodentate binding of a MN_2S_2 metalloligand is also available (Figure 2A-B). Some noble features of the MN_2S_2 class of metalloligands include: (1) the square planar binding conformation of the N_2S_2 donor set; (2) ability to modify the M−S−C−N and/or M−N−C−N ring size by adjusting the number of C atoms;

(3) ability to change the overall ligand charge.[5] These features make this type of metalloligands flexible to adjust steric, electronic, and photochemical properties for different applications.

MN_2S_2 vs. bipyridine as redox-active ligands in heterobimetallic complexes to serve as a receptor and conduit of electrons

In 1984, Hawecker, Lehn, and Ziessel introduced the first evidence of electrocatalytic activity for the reduction of CO_2 to CO of metal carbonyl complexes by the pioneering fac-Re(bpy)(CO_3)Cl (bpy = 2,2-bipyridine) compound.[10] Although studies about Lehn's catalysts were extensively carried out by Kubiak and coworkers in efforts to understand the mechanism and improve the catalytic properties, their modifications only focused on substitutions on the 4,4'position of the bipyridine ligand in Re complexes.[11,12] It was not until 2011 that the first analogous manganese carbonyl complexes, fac-Mn(bpy)(CO_3)Br and fac-Mn(dmbpy)(CO_3)Br, were reported by Bourrez and coworkers.[13] However, a single-electron addition to the Bourrez's catalysts followed by the loss of Br- leads to a rapid irreversible dimerization which limits the catalytic activity and is not seen in the rhenium counterparts.[14] Advances in both eliminating the dimerization and enhancing CO_2 reduction catalytic activity in the last 8 years have resulted from incorporating innovative bulky substituents on the bipyridine ligand (Figure 3). Manipulation of the secondary coordination sphere with functional group moieties such as ether, imidazolium, amine, phenol, etc. added to the progress.[15-18] However, the story of manganese carbonyl diimine catalysts is only in its infancy since most of recent work just examines modifications of the bipyridine ligand; while expanding to another redox active ligand has not been investigated in our knowledge.

Inspiration for such types of ligand can be seen in biological systems, especially in natural metalloenzymes as discussed above. However, there is little exploration of these ligands to be

found toward CO_2 reduction catalysts. In 2017, Darensbourg and coworkers built the connection between bio-inspired ligands and manganese carbonyl catalysts by the synthesis of a class of stable, electron-rich bimetallic complexes featuring MN_2S_2 metallodithiolates, with M = Ni^{2+}, $\{Fe(NO)\}^{2+}$, and $\{Co(NO)\}^{2+}$, bound to $M'(CO)_3X$, where M' = Mn and Re (Figure 4).[9] Due to the variety and the versatile binding ability of the N_2S_2 class of ligands, the structural and electronic properties of complexes with these ligands become unpredictable, yet fascinating to researchers. However, the CO_2 reduction catalytic ability of the complexes has not been discovered.

[(*ema*)M]$^{2-}$ metalloligands as electron-rich versions of MN_2S_2 for better catalytic activity

The loss of bromide is the critical step to the catalysis mechanism for CO_2 reduction (Figure 5).[11,12,19] In order to make the bromide leave the system more easily, an anionic should be used in alternative for neutral MN_2S_2 ligands in similar heterobimetallic complexes. Here, $[(ema)H_2]^{2-}$ (*ema* = N,N'-ethylenebis(mercaptoacetamide)) has been used for advances to combine the natural bioorganometallic chemistry and commercial catalysts (Figure 6).[20] Bearing a metal ion, complexes of the $(ema)^{4-}$ ligand were wished to have better catalytic activities than the previous heterobimetallic complexes of MN_2S_2.

Application of coordination complexes of Mn, Re, and Fe

There are many reasons that Mn is chosen for electrocatalysis albeit it may not be found in biological systems as often as Ni or Fe. Manganese carbonyl catalysts captured much attention due to the greater abundance of manganese than rhenium in Earth's crust and the lower overpotentials for the reduction of CO_2 to CO as compared to the corresponding rhenium catalysts. Using Mn compounds as an inexpensive starting material to prepare CO_2 reduction catalysts has been the most common trend in the past two decades. Being in the same group as Mn, Re has its own area

of applications in radiopharmaceuticals.[21,22] Since it is well-known that Mn and Re can be substituted for each other and Re has a greater binding force to substrates than Mn, it is surmised that Re would react analogously with $(ema)^{4-}$ ligand to that of Mn.

Our interest in Fe is inspired by the organometallic active site of the diiron hydrogenase enzyme ([FeFe]-H_2ase), which is a remarkable catalyst for H_2 production. Its ersatz small-molecule mimics have been heavily studied in the last two decades and shown evidence of regioselectivity in ligand substitution.[23] Similarities between these synthetic analogues of the 2Fe subsite of the [Fe-Fe]-H_2ase active site and the $[Mn(CO)_3]_2(H_2ema)$ include the bimetallic centers system, the three CO ligands binding each metal center, and two thiolates metal bridges. The replacement of Mn centers by Fe would advance our exploration in study of bio-inspired organometallic complexes.

An unprecedented result

In attempts to further explore the bimetallic complex featuring redox active MN_2S_2 metallodithiolates ligands, we have synthesized a novel bimetallic manganese complex bearing the bio-inspired ema ligand – a model of the tripeptide Cys-Gly-Cys found in acetyl CoA synthase.[24] The X-ray diffraction study of $[Mn(CO)_3]_2(H_2ema)$ indicates the first example of ema^{4-} acting as a binucleating S_2O_2 ligand instead of N_2S_2 to a single metal as in previously reported $Ni(ema)^{2-}$ and $(V{=}O)(ema)_{2-}$. In addition, different preparation methods for $[Mn(CO)_3]_2(H_2ema)$ elucidated an unusual metal templating effect that facilitates the formation of this structure. Because the structure of $[Mn(CO)_3]_2(H_2ema)$ complex presents several potential features such as its amido carbonyl bonding lability, metal centers bridged by two thiolates, and an acidic proton on nitrogen, the elucidation of the properties of this new structure has become an attractive goal

for our research. Moreover, the Re analogue of $[Mn(CO)_3]_2(H_2$*ema*$)$ were also synthesized and the Fe analogue has been in its preparation progress.

CHAPTER II

EXPERIMENTAL SECTION

General procedures and physical methods

All manipulations involving air-sensitive compounds were carried out with the standard Schlenk/syringe rubber septa techniques under N_2 gas and/or glovebox techniques under N_2/Ar unless otherwise noted. Solvents were reagent grade, purified according to procedures, and freshly distilled under nitrogen gas prior to use.

All infrared spectra were recorded on a Bruker Tensor 37 spectrometer in a NaCl solution cell of 0.2 mm path length. Electron spray ionization mass spectrometry measurements were performed by faculties at the Laboratory for Biological Mass Spectrometry, Texas A&M University, College Station, Texas. ^{1}H-NMR and ^{13}C-NMR spectra were recorded using a Bruker Avance III 400 MHz Broadband spectrophotometer operating at 400.1 MHz and an Inova 500 MHz spectrophotometer operating at 125.6 MHz, respectively. Data for single crystal structure determination were collected at 110K using a Bruker D8 Quest with graphite monochromated Mo radiation source (λ = 0.710731 Å) or a Bruker Apex2 with CCD area detector. All crystals were coated with paraffin oil and mounted on a MiTeGen microloop. Graphical representations were generated using Olex2 software package.

Materials

Acetic acid (CH_3COOH, Fisher Chemical, ACS Reagent grade); acetonitrile (MeCN, EMD Chemicals Inc., >97%); diethyl ether ($(C_2H_5)_2O$, EMD Chemicals Inc., >97%); ethanol (MilliporeSigma, 98%); hexane (Fisher Chemical, 99.9%); trimethylamine N-oxide ((CH3)3NO, Alfa Aesar, 98%); manganese pentacrbonylbromide (Sigma Aldrich, 98%); sodium

hydroxide (pellets, EMD Millipore); tetraethyl ammonium chloride (Alfa Aesar, >98%); vanadium (IV) sulfate oxide hydrate (Alfa Aesar, 98%), zinc oxide (ARCOS Organics, 99%), ethylenediamine (Fisher Chemicals, 99%), pyridine (Sigma Aldrich, 98%), and other reagents were purchased, stored under an inert atmosphere, and used as received unless otherwise noted.

Syntheses

[fac-Mn(CO)3]2[κ3-κ3'-μ2S-μ2S'-O,O'-(N,N'-ethylenebis(2-mercaptoacetamide)] ***(Compound 1)***

Method 1 (Metal templating)

A mixture of $[M(ema)][NEt_4]_2$ (M=Ni, V=O, or Fe, 0.13 mmol), $Mn(CO)_5Br$ (52 mg, 0.19 mmol) and acetic acid (0.01 mL, 0.2 mmol) in 15 mL of MeOH were stirred at 60°C a under N_2 stream, in dark for 12h. The amount of MeOH was reduced to minimum and excess Et_2O was added from which the by-product precipitated. The resulting yellow solution was filtered through Celite and brought to dryness under vacuum yielding light yellow solid product. Vapor diffusion of pentane into the THF solution produced pure orange X-ray quality crystals. Spectroscopic yield: 82% (39% if HOAc was not used). IR data in THF (ν_{CO}, cm^{-1}): 1915 (br,s), 2006(s), 2025 (m); ^1H – NMR (ppm) in CD3CN: 7.97 (br, 2H), 4.09 (m, 2H), 3.08 (d, 2H), 2.99 (d, 2H), 2.97 (m, 2H); ^{13}C – NMR (ppm) in DMSO: 35.8, 42.3, 182.3 (amide C=O) 215.4 (CO), 216.7 (CO) and 225.4 (CO); ESI-MS(-) (m/z): 482.85 $[M-H]^-$.

Method 2 (Metal templating in situ)

A mixture of *'ema'* ligand (50 mg, 0.17 mmol, 1 eq.) and NaOH (14 mg, 0.35 mmol, 2 eq.) in 5 mL of MeOH was stirred for 15 min, following by an addition of 5 mL of a methanolic solution of $Zn(OAc)_2$ (32 mg, 0.17 mmol, 1 eq.) resulting in a cloudy solution. Immediately after this, $Mn(CO)_5Br$ (95 mg, 0.34 mmol, 2 eq.) in 15 mL of MeOH was cannula transferred to the

reaction mixture following by stirring at 60°C under a gentle N_2 stream in the absence of light. After the completion of the reaction was confirmed by FTIR after 3 h, the methanol solvent was evaporated under vacuum. The orange residue was extracted into 15 mL of THF and anaerobically filtered. The THF solvent was removed in vacuo and the orange residue was freeze dried to yield 84 mg (94 %). Vapor diffusion of pentane into a saturated solution of the complex in THF produced X-ray-quality orange blocky crystals after 3 days. FTIR (THF): 2025 (w), 2006 (s), 1915 (s), 1611 (m) cm^{-1}. ESI-MS (THF): *m/z* 483. ^{1}H – NMR (ppm) in CD_3CN: 7.97 (br, 2H), 4.09 (m, 2H), 3.08 (d, 2H), 2.99 (d, 2H), 2.97 (m, 2H); ^{13}C – NMR (ppm) in DMSO: 35.8, 42.3, 182.3 (amide C=O) 215.4 (CO), 216.7 (CO) and 225.4 (CO).

Method 3 (Direct synthesis B)

A mixture of protected '*ema*' ligand (10 mg, 0.035 mmol) and NaOH (3 mg, 0.07 mmol) in 5 mL of MeOH was stirred for 15 min generating H_2ema^{2-}, to which 5 mL of MeOH solution containing $Mn(CO)_5Br$ (19 mg, 0.07 mmol) was added. The mixture was stirred at 60°C, in dark for 12h. Work – up procedure is the same as the Method 1. Spectroscopic yield was determined to be 50%.

Method 4 (Direct synthesis A)

A mixture of protected '*ema'* ligand (10 mg, 0.035 mmol) and NaOH (8.4 mg, 0.21 mmol) in 15 mL of MeOH was stirred for 15 min to which 5 mL of MeOH solution containing $Mn(CO)_5Br$ (19 mg, 0.07 mmol) was added. The mixture was stirred at 60°C, in dark for 12h. Work – up procedure is the same as the Method 1. Spectroscopic yield is less than 10%.

CO exchange reactions

A 30 mL solution containing 20 mg of complex 5 in either MeOH, THF or DMSO – d_6 in a 100-mL Schlenk flask was degassed using 3 cycles of freeze-pump-thaw. The flask was then

filled with a slight overpressure of ^{13}CO, wrapped in aluminum foil, and the exchange/enrichment was monitored by FT-IR spectroscopy. The generated ^{12}CO concentration was partially removed and the ^{13}CO was replenished by syringes for every 4-5 h. After 4 days, an aliquot was taken out from the solution, brought to dryness under vacuo, and the resulting enriched product was dissolved in DMSO-d_6. The ^{13}C – NMR spectrum was then taken.

*[fac-Re(CO)3]2[κ3-κ3'-μ2S-μ2S'-O,O'-(N,N'-ethylenebis(2-mercaptoacetamide)] (Compound **2**)*

A mixture of protected '*ema'* ligand (50 mg, 0.17 mmol) and KOH (19 mg, 0.34 mmol) in 5 mL of MeOH was stirred for 15 min, to which 5 mL of MeOH solution containing $Zn(OAc)_2$ (38 mg, 0.20 mmol) and $Re(CO)_5Cl$ (124 mg, 0.34 mmol) was added. The reaction mixture was heated and stirred at 60 ^oC under a gentle stream of N_2. Upon completion, the colorless solution was brought to dryness under vacuum and the white solid residue was treated with 5 mL of THF. The THF solution was filtered through Celite and evaporated to yield the crude product, which was then purified by a series of filtration in minimum amount of MeCN. FTIR (THF, cm^{-1}): 2025 (m), 2010 (s), 1902 (s), 1608 (m). ESI-MS (THF): m/z 744.89. ^{13}C–NMR (DMSO, δ,ppm): 196.7, 196.1, 193.3.

$Fe(CO)_4X_2$

A solution of $Fe(CO)_5$ (5 mL, 38 mmol) in THF (40 mL) and a solution of X_2 (I: 9.0 g, 35 mmol, Br: 5.6 g, 35 mmol) in THF (50 mL) were added dropwise into a flask. The flask was cooled by emerging in an ice-water bath. The reaction solution bubbled vigorously and the light-yellow color (when using I_2) changed dark red. The reaction was allowed to stir for 20 min. The volume of the solvent was reduced to minimum by vacuum. Petroleum ether (50 mL) was added and a dark red crystalline solid was precipitated. The product ($[Fe(CO)_4I_2]$) was collected and washed with 20 mL of petroleum ether.

[fac-Fe(CO)3]2[κ3-κ3'-μ2S-μ2S'-O,O'-(N,N'-ethylenebis(2-mercaptoacetamide)]

Method 1

A mixture of the crystalline $[Fe(H_2ema)]_2$ (20 mg, 0.04 mmol) and $Fe(CO)_4I_2$ (31 mg, 0.08 mmol) in 15 mL of THF was stirred at -35 ^oC in an ice bath under N_2 stream, in dark. The compound decomposed after 12 h. FTIR (THF, after 1 h, ν_{CO}, cm^{-1}): 2070 (m), 2017(br, s), 1994 (m).

Method 2

A mixture of the $Fe(CO)_4I_2$ (64 mg, 0.08 mmol) and $(VO)(H_2ema)$ (20 mg, 0.08 mmol) in 15 mL of THF was stirred at -78 ^oC in an cooling bath of dry ice and acetone under N_2 stream, in dark. The solution was stirred and was monitored by infrared spectroscopy. The compound decomposed after 3 days. FTIR (THF, after 1 h, ν_{CO}, cm^{-1}): 2135 (m), 2087 (br, s), 2073 (w).

Compound 3

A mixture of $Mn(CO)_5Br$ (0.1 g, 0.36 mmol), methyl mercaptoacetate (0.03 mL, 0.36 mmol) and Et_3N (0.05 mL) in CH_2Cl_2 (20 mL) was stirred at room temperature for 4 h, by which time bands in IR spectra from $Mn(CO)_5Br$. FTIR (THF, after 4 h, cm^{-1}): 2055 (s), 2000 (w), 1990 (s), 1732 (s).

2-mercapto-N-methylacetamide

A mixture of methylamine hydrochloride (0.68 g, 10.0 mmol), sodium methoxide (0.54 g, 10.0 mmol) in methanol (25 mL) was stirred at room temperature for 1 h. The volume of the solvent was reduced to minimum and diethyl ether was added. The white suspension was filter through Celite to give a colorless solution. Diethyl ether was removed by vacuum and the solid was re-dissolved in methanol. Methyl mercaptoacetate (0.4 mL, 4.5 mmol) was added and the colorless solution was stirred over night at room temperature.

*Compound **4***

A mixture of $Mn(CO)_5Br$ (0.27 g, 1.0 mmol) and 2-mercapto-N-methylacetamide (0.12 mg, 1.1 mmol) and Et_3N (0.15 mL) in CH_2Cl_2 (20 mL) was stirred at room temperature for 4 days and the reaction was monitored with infrared spectroscopy. FTIR (THF, after 4 days, cm^{-1}): 2079 (w), 2050 (m), 2010 (s), 1958 (m), 1925 (m), 1732 (w), 1676 (w), 1618 (w).

Deprotonation reactions

Solid sodium hydride (0.8 mg, 0.04 mmol) or sodium methoxide (1.5 mg, 0.03 mmol) was added to a solution of $[Mn(CO)_3]_2(H_2$*ema*$)$ (5 mg, 0.01 mmol) in THF (5 mL). The orange solution was stirred, and the reaction was monitored using infrared spectroscopy. The solution turned slightly green after 5 min and then turned orange. After 90 min, the suspension was filtered through Celite to give a clear orange solution. FTIR (THF, cm^{-1}): 2008 (m), 1973 (s), 1908 (s), 1886 (s), 1848 (m).

CHAPTER III

$H_2(ema)^{2-}$ AS A BINUCLEATING LIGAND WITH BRIDGING SULFURS AND CARBOXAMIDE OXYGENS TO Mn AND Re

Metal templating effect

Compound **1** can be obtained from several synthetic methods displayed in Figure 1.

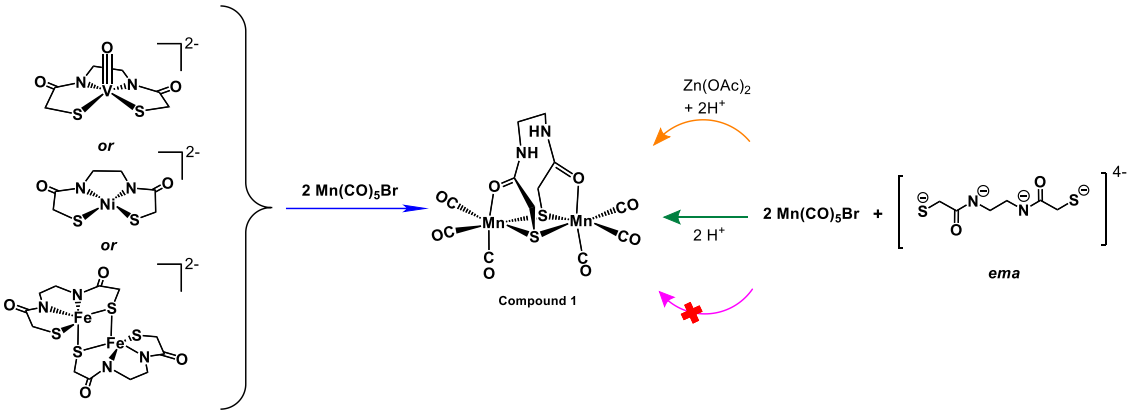

Figure 1. Synthesis routes for compound **1** (Metal templating: blue, metal templating in situ: orange, direct syntheses: pink and green)

Initially, compound **1** was initially isolated from an overnight reaction of $[(ema)V{=}O](Et_4N)_2$ and 2 equivalents of $Mn(CO)_5Br$ in a MeOH solution at 60°C under an inert atmosphere. The same product was achieved when $Ni(ema)^{2-}$ or dimeric $Fe(ema)^{2-}$ was used in replacement of vanadyl$(ema)^{2-}$. Usually, reactions between $M(CO)_5X$ (M = Mn and Re) with $M'N_2S_2$ metallodithiolate ligands would result in butterfly type structures of heterobimetallic complexes as Darensbourg and coworkers reported.[9] To pur best knowledge, this is our first observation that the metal originally resided inside the N_2S_2 pocket is removed to rise to the formation of the S_2O_2 binucleating tridentate ligand. Attempts to directly synthesize compound **1** without adding a metal source by reacting 2 equivalent of $Mn(CO)_5Br$ with different deprotonation levels *ema* ligand

(*ema*$^{4-}$ and H_2*ema*$^{2-}$) with different amounts of NaOH were unsuccessful to yield pure isolated product and crystals. However, with the presence of a stoichiometric amount of $Zn(OAc)_2$, the reaction of $Mn(CO)_5Br$ with H_2*ema*$^{2-}$ was accomplished in only 3 hours and yielded large blocky crystals of compound **1** co-crystallized with $ZnBr_2$. We suggest that the role of a metal ion is essential for the synthesis because the backbone of '*ema*' ligand needs to be folded before the addition of $Mn(CO)_5Br$ in order to form an unprecedented binucleating form of '*ema*' ligand. We suppose that zinc is the prime candidate since it can quickly fill into the N_2S_2 pocket within minutes while the mostly ionic interaction of zinc with the ligand are weak enough that the templated ligand can be efficiently transferred to the manganese centers. Following this metal templating in situ method, compound **2**, which is the Re analogue of compound **1**, was also prepared.

Several attempts to synthesize $[Fe(CO)_2I]_2$(H_2*ema*) were made but unsuccessful due to the low stability of Fe complexes. Firstly, the starting material $Fe(CO)_4X_2$ (X = Br or I) was prepared. Because $Fe(CO)_4Br_2$ was unstable and decomposed, $Fe(CO)_4I_2$, which was made by adding dropwise $Fe(CO)_5$ and I_2 into each other in THF at < 0 ^oC, was then used to synthesize $[Fe(CO)_2I]_2$(H_2*ema*) in two ways: reaction with the dimeric Fe(H_2*ema*) and reaction with vanadyl *ema* (3). The reaction of $Fe(CO)_4I_2$ with Fe(H_2*ema*) was carried out under N_2 atmosphere, in THF and at -35 ^oC. Monitoring the reaction by IR showed that all signals of the starting material red-shifted significantly which proved that the reaction happened. However, the compound decomposed overnight, which was indicated by a disappearance of a CO peak in the IR. To overcome the low stability of Fe(H_2*ema*) compounds, another attempt was made using 3 as the source of *ema* ligand. The reaction was carried in the same condition except at about -78 ^OC in a cooling bath of dry ice and acetone. The reaction was also monitored using IR spectroscopy. The IR spectrum after 1 h of the reaction showed a continuing shifting at 2080 cm^{-1}. However, after

letting stirred overnight at low temperature, the none of the expected peaks appeared which indicate the decomposition of the compound. Since the first attempt showed that the reaction occurred but was hindered by the low thermal stability of the Fe species, further studies of this synthesis will focus on controlling the stability and monitoring the reaction at different temperature.

Characterization and properties of M(H_2*ema*), (M = Mn and Re)

Complexes **1** and **2** are soluble in H-bonding acceptor solvents (MeOH, THF, acetone, DMSO, and Et_2O), sparingly soluble in nonpolar hydrocarbons, CH_3CN, and CH_2Cl_2, and insoluble in water. Remarkably, the solid **1** showed a very high thermal stability (decomp. pt. > 250 ^oC and stable in toluene upon refluxing for 6 h), which is based on the ability to form H-bonding by the protonation at the amide nitrogens. Solution infrared spectrum of **1** and **2** in methanol showed three ν(CO) bands that are assigned based on the C_2 symmetry of the structures (Figure 2).

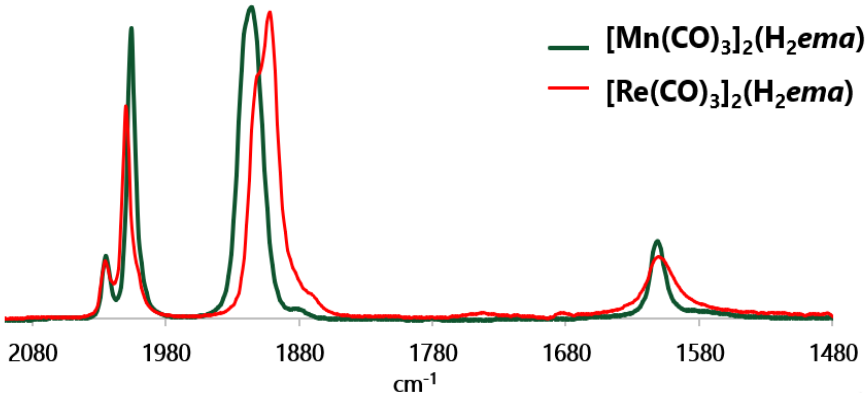

Figure 2. FT-IR spectra of complexes **1** and **2**

Natural abundance ^{13}C-NMR of complex **1** show expected signals at 35.8, 42.3, 182.3 ppm for amide C=O and 215.5, 216.7, 225.4 for CO (Figure 3 top). The ^{13}C-NMR also confirms the C_2

symmetry of the molecular structure of **1** and indicates that the chemical environments of each facial CO around the metal center are not equivalent.

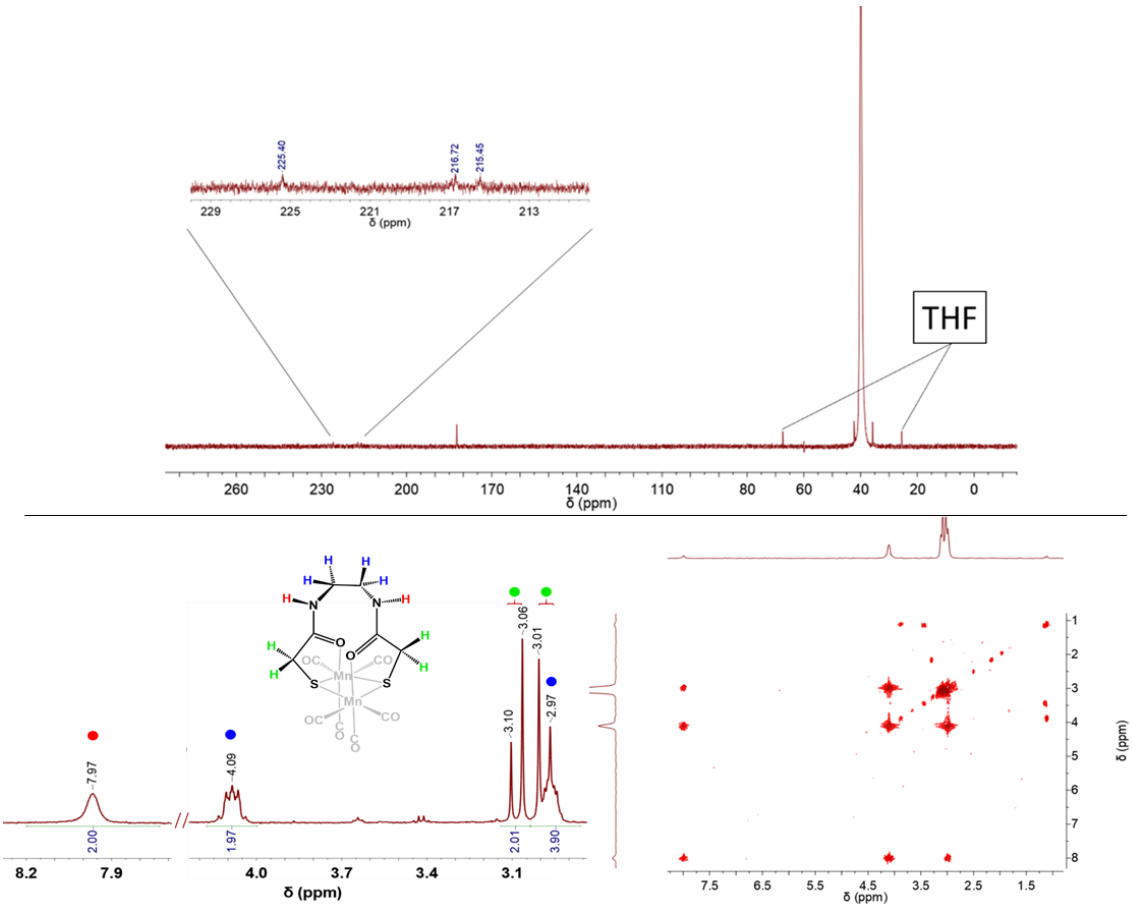

Figure 3. Natural abundance 13C – NMR of **1** in DMSO-d_6 with the carbonyl region magnified (top). COSY–NMR (bottom right) and ^{1}H-NMR (bottom left) spectra of **1** in CD_3CN.

Signals of the ^{1}H-NMR and COSY spectra of **1** in CD_3CN (Figure 3) were assigned that the resonance at 8.0 ppm represents the amide protons (2H); the multiplet at 4.1 ppm (2H) and the signal at 3.0 represent the protons of the carbons adjacent to the nitrogens; and the group signal from 3.0–3.1 ppm represent the protons of carbons adjacent to sulfurs. The ESI-MS spectra of compound **1** and **2** were recorded in THF (Figure 4). The spectrum for **1** showed a peak of high intensity centered at m/z = 482.8573 consistent with the information for $C_{12}H_{10}Mn_2N_2O_8S_2$.

Another noticeable peak at 528.861 suggests the formation of **1** and a formate ion which alludes to an unknown mechanism that happened during the reaction. Mass spectrometry spectrum of **2** also showed the expected signal at 744.8908 for $C_{12}H_{10}Re_2N_2O_8S_2$.

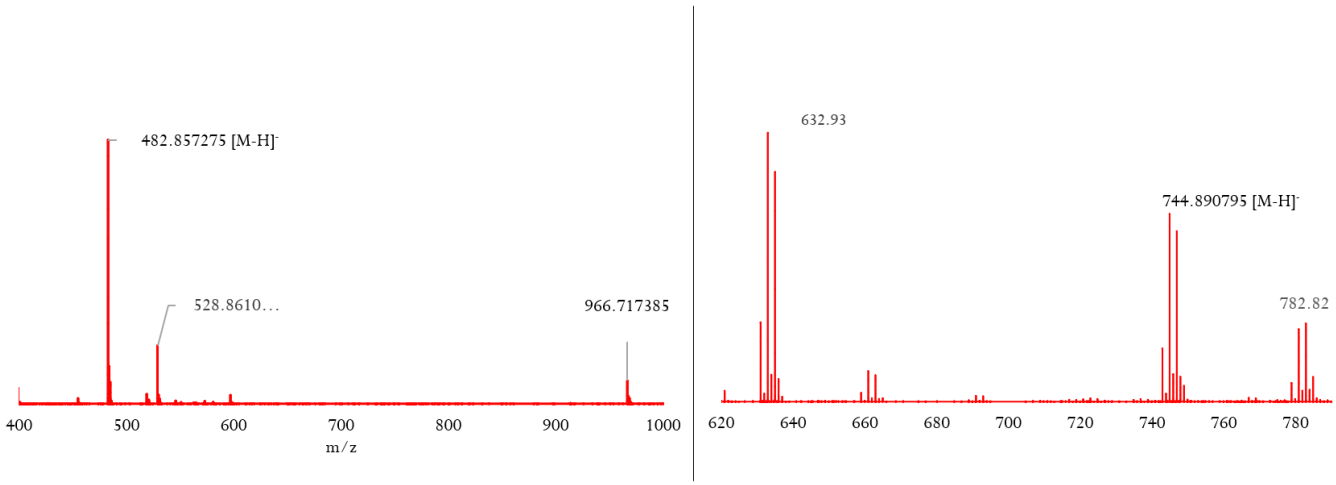

Figure 4. ESI-HRMS negative mode spectra of **1** (left) and **2** (right)

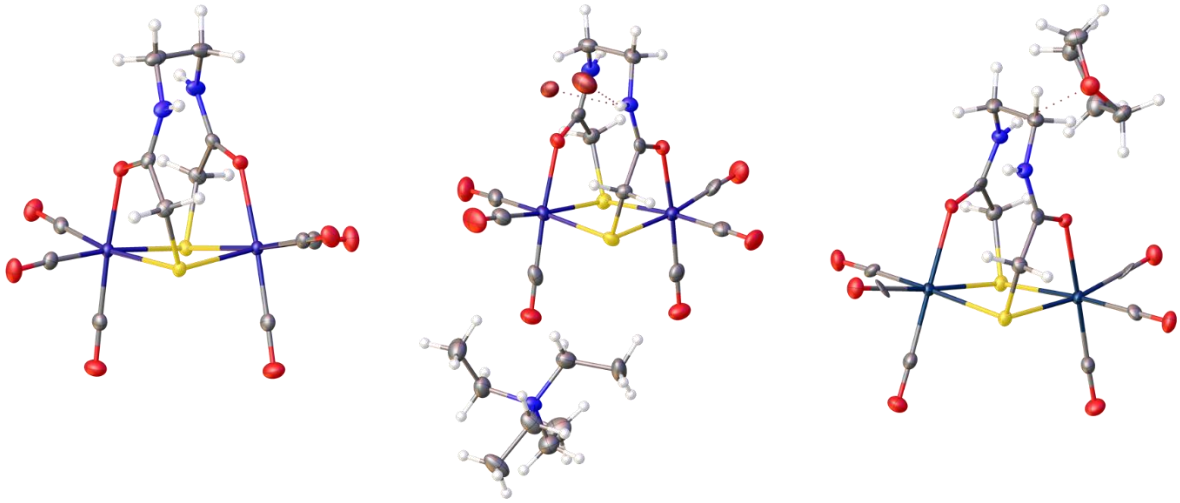

Figure 5. Crystal structures of **1** (left and middle) and **2** (right)

X-ray crystallography was used to figure the crystal structures of **1** and **2** (Figure 5). Figure 5 middle shows **1** co-crystallized with Et_4NBr and f]Figure 5 right shows **2** co-crystallized with THF. Crystals of **1** and **2** were grown by vapor diffusion of pentane into a THF solution of the complexes.

Both complexes crystallize in the monoclinic C2/c space group while crystals from co-crystallization is in the P21/c space groups. Crystals collected from the Zn^{2+} templated reactions are giant blocks (> 3 mm), while the ones from other synthetic methods are small. Differences between these two crystal structures are minute. Geometry of both crystals was determined as pseudo-octahedral around each metal center. Each center is coordinated by 2 bridging sulfurs, 3 carbonyls and one carboxamide oxygen. In both compounds, the *ema* ligand coordinates to the equivalent metal centers in a facial SS'O mode through two bridging sulfurs. In addition, an oxygen atom allows the octahedral sites on the M(I) centers to be completed with three CO's. Two five-membered M-S-CH_2-C-O rings, in which metal centers reside both hard and soft ligand donor sites, achieved by only one ligand is unprecedented. A related Mn_2S_2 motif, where a bidentate ligand also features both of hard and soft donors, has observed earlier by Nicholson and coworkers,[25] but the two five-membered, Mn-μ-S-CH_2-C-O, rings are in the opposite positions. Intermolecular hydrogen bonds were also observed for all three crystals. Moreover, as the ∠N-H-Br is 166.1° and the N-Br distance of 3.25 Å, N-Br bonds in **1** and **2** can be also categorized as moderate H-bonds. In the crystal **3**, which co-crystallized with THF, the bond between the oxygen atom of THF and the proton of the closest nitrogen is 2.093 Å. The M-C-O angles vary from 175.5° to 178.9°. This range is broader than those observed in the Re/Mn diimine carbonyl compounds (177.3° and 178.4°)[9] and the bimetallic complexes with MN_2S_2 ligands (177.1° to 178.6°)[9]. The distance between two manganese centers is 3.5662 Å and between two rhenium centers is 3.7960 Å, which are greater than all M-M' distances in Darensbourg's reported complexes.[9] The bond distances in 2 are generally greater than those corresponding distances in 1, which suggest that the dirhenium compound may be less stable than its Mn model. Intermolecular hydrogen-bondings of S and H are also seen in the neutral complexes with a distance around 2.5 Å. Bond lengths

comparison between 1 and 2 can be found in table 1. Other elected metric data and experimental crystallographic data of complexes **1**, **1** co-crystallized with Et_4NBr, and **2** are given in Tables 2, 3, and 4 and Figure 6, 7, and 8.

Table 1. Bond lengths comparison between complexes **1** and **2**

Distances (Å)	$[Re(CO)_3]_2(H_2ema)$	$[Mn(CO)_3]_2(H_2ema)$
M–M	3.7960(4)	3.5662(4)
M–S	2.4914(18), 2.5252(17)	2.3628(4), 2.4014(4)
M–C	1.892(8) – 1.917(8)	1.7864(14) – 1.8225(14)
M–O	2.190(5)	2.0725(9)
$C–O_{carbonyl}$	1.139(10) – 1.514(10)	1.1436(17) – 1.1512(18)

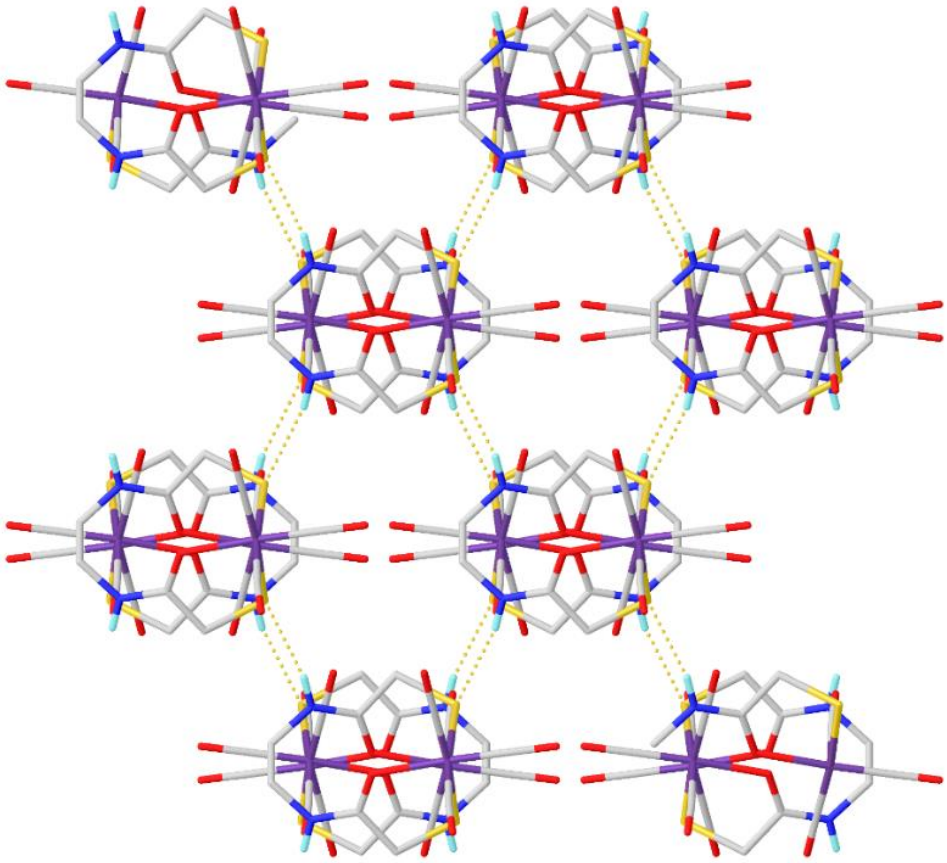

Figure 6. Packing diagram of **1** with dotted lines represent H-bonds.

Table 2. Crystal data and structure refinement for **1**

Empirical formula	$C_{12}H_{10}Mn_2N_2O_8S_2$
Formula weight	484.22
Temperature/K	110.0
Crystal system	monoclinic
Space group	C2/c
a/Å	11.8954(3)
b/Å	10.1970(3)
c/Å	14.1602(4)
α/°	90
β/°	98.2190(10)
γ/°	90
Volume/Å^3	1699.95(8)
Z	4
ρ_{calc}g/cm^3	1.892
μ/mm^{-1}	1.776
F(000)	968.0
Crystal size/mm^3	0.2 × 0.1 × 0.1
Radiation	MoKα (λ = 0.71073)
2Θ range for data collection/°	7.484 to 60.084
Index ranges	$-16 \leq h \leq 16$, $-14 \leq k \leq 14$, $-19 \leq l \leq 19$
Reflections collected	33874
Independent reflections	2472 [R_{int} = 0.0320, R_{sigma} = 0.0122]
Data/restraints/parameters	2472/0/118
Goodness-of-fit on F^2	1.110
Final R indexes [I>=2σ (I)]	R_1 = 0.0204, wR_2 = 0.0507
Final R indexes [all data]	R_1 = 0.0245, wR_2 = 0.0552
Largest diff. peak/hole / e Å^{-3}	0.38/-0.39

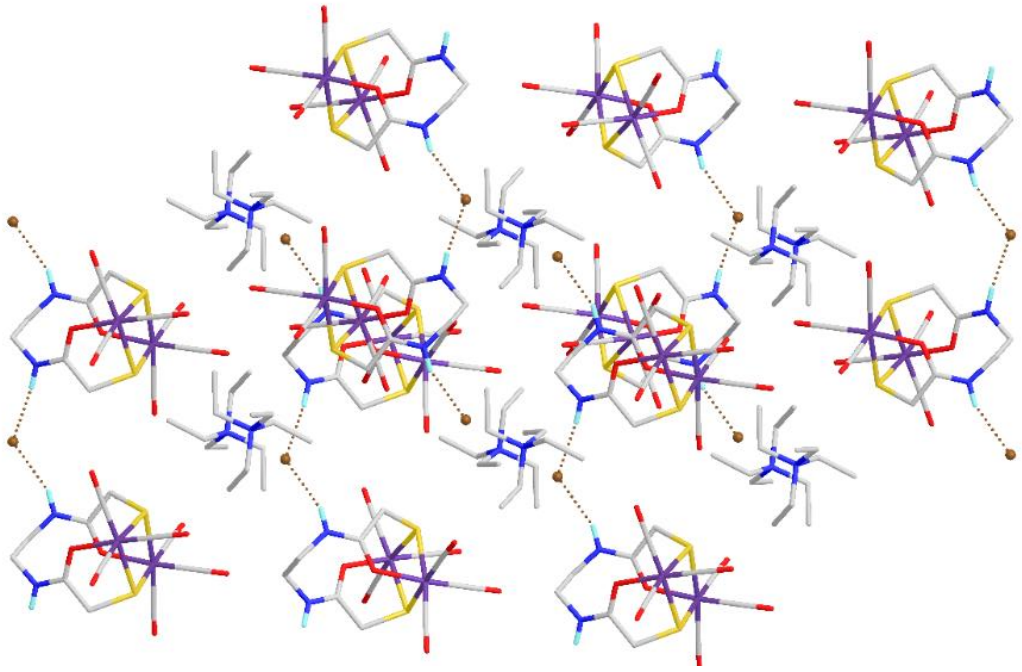

Figure 7. Packing diagram of **1**-Et_4NBr with dotted lines represent H-bonds.

Table 3. Crystal data and structure refinement for **1**-Et_4NBr

Empirical formula	$C_{20}H_{30}BrMn_2N_3O_8S_2$
Formula weight	694.38
Temperature/K	110
Crystal system	monoclinic
Space group	$P2_1/c$
a/Å	8.2438(10)
b/Å	16.986(2)
c/Å	20.496(3)
α/°	90
β/°	93.663(3)
γ/°	90
Volume/$Å^3$	2864.1(6)
Z	4
$\rho_{calc}g/cm^3$	1.610
μ/mm^{-1}	2.468
F(000)	1408.0

Table 3. Crystal data and structure refinement for **1**-Et_4NBr (Continued)

Crystal size/mm^3	0.2 × 0.1 × 0.1
Radiation	MoKα (λ = 0.71073)
2Θ range for data collection/°	3.116 to 54.65
Index ranges	$-10 \leq h \leq 10$, $-21 \leq k \leq 21$, $-26 \leq l \leq 26$
Reflections collected	70131
Independent reflections	6413 [R_{int} = 0.1482, R_{sigma} = 0.0795]
Data/restraints/parameters	6413/0/339
Goodness-of-fit on F^2	1.047
Final R indexes [I>=2σ (I)]	R_1 = 0.0540, wR_2 = 0.0939
Final R indexes [all data]	R_1 = 0.1029, wR_2 = 0.1070
Largest diff. peak/hole / e $Å^{-3}$	0.84/-0.51

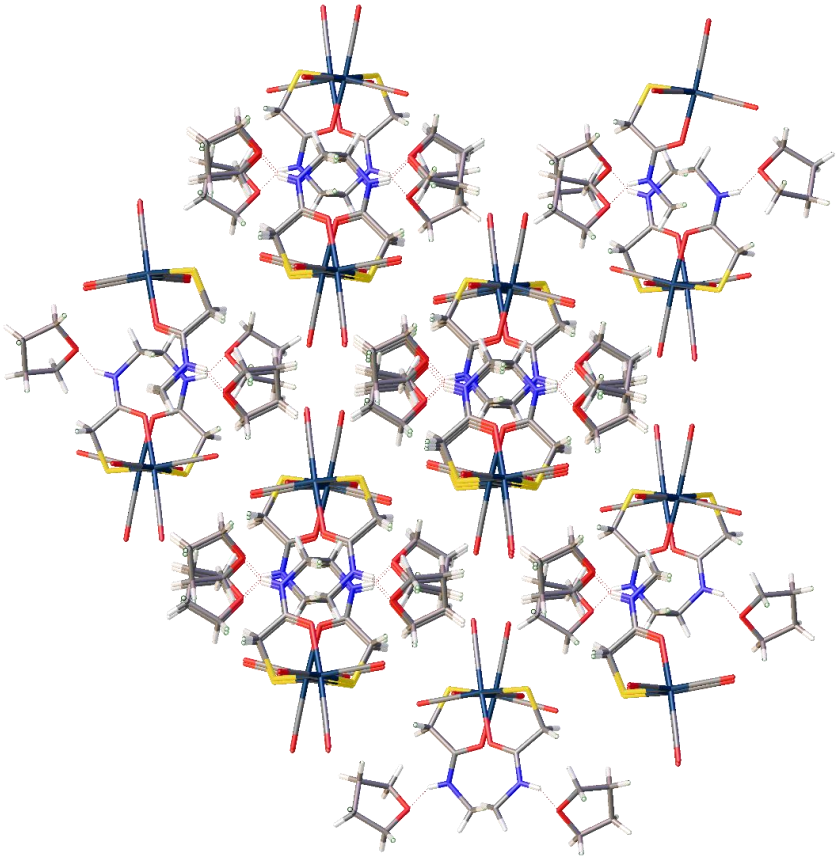

Figure 8. Packing diagram of **2** with dotted lines represent H-bonds

Table 4. Crystal data and structure refinement for **2**

Empirical formula	$C_{10}H_{13}NO_5ReS$
Formula weight	445.47
Temperature/K	110.0
Crystal system	monoclinic
Space group	C2/c
a/Å	16.7531(16)
b/Å	16.6772(16)
c/Å	10.6775(10)
α/°	90
β/°	120.824(2)
γ/°	90
Volume/Å^3	2561.8(4)
Z	8
ρ_{calc}g/cm^3	2.310
μ/mm^{-1}	9.661
F(000)	1688.0
Crystal size/mm^3	? × ? × ?
Radiation	MoKα (λ = 0.71073)
2Θ range for data collection/°	5.664 to 60.192
Index ranges	$-23 \leq h \leq 23$, $-23 \leq k \leq 23$, $-15 \leq l \leq 15$
Reflections collected	31274
Independent reflections	3770 [R_{int} = 0.0471, R_{sigma} = 0.0249]
Data/restraints/parameters	3770/0/163
Goodness-of-fit on F^2	1.398
Final R indexes [I>=2σ (I)]	R_1 = 0.0351, wR_2 = 0.0917
Final R indexes [all data]	R_1 = 0.0498, wR_2 = 0.1188
Largest diff. peak/hole / e Å^{-3}	6.30/-4.36

CHAPTER IV

REACTIVITIES OF $Mn_2(H_2ema)$

CO ligands exchange experiments

As mentioned in the NMH study, the CO ligands in compound **1**are not chemically equivalent; therefore, we conducted $^{13}CO/^{12}CO$ exchange reactions to study their chemical heterogeneity. These experiments were carried with the method mentioned in the experimental section. The reactions were monitored by FT-IR and ^{13}C-NMR spectroscopies (Figure 9). The ^{13}C-NMR spectra (Figure 9 right) clearly indicate that the resonance intensities of the CO signals increased at the same rate when the reaction was run in MeOH, while the rates are varied for the reactions in THF and DMSO.

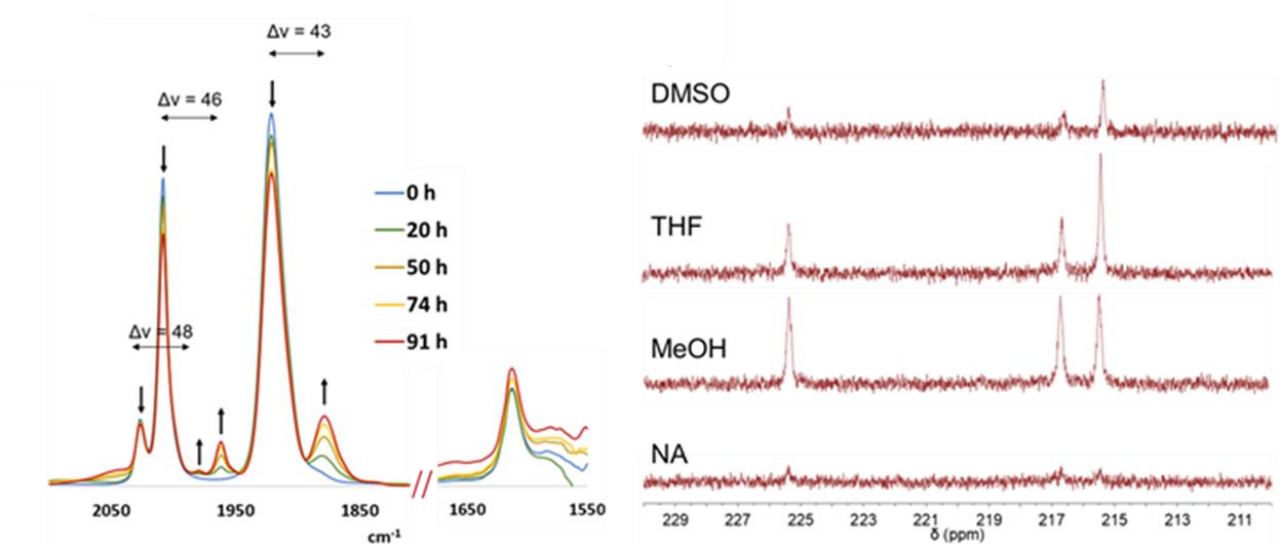

Figure 9. FT-IR spectra of **1** under ^{13}CO at 1 atm in MeOH (left) and stacked ^{13}C-NMR spectra in DMSO-d_6) of **1** isolated from partial ^{13}CO enrichment in different solvents.

The rate difference also suggests that the CO that accounts for the signal around 215.4 ppm in the ^{13}C-NMR spectra has a different exchange behavior from the other two CO ligands. Since the

polarities of DMSO and MeOH are close to each other, the solvent dependence of the exchange reactions cannot be explained by solvent polarities. On the other hand, unlike DMSO and THF, MeOH can act as both H-bond acceptor and donor that could induce a dual H-bond effect to complex **1**. The assignments for which CO ligand exhibits the highest resonance increasing rate will be discussed in later reports.

Deprotonation reaction of compound $Mn_2(H_2ema)$

Since Mn^I hydrogenation catalysts have caught attention of chemists in the past five years, we are interested to know if compound **1** is hydrogenation catalytically active. From the structure of **1**, we expect that **1** could be activated for catalysis if the nitrogen atoms are deprotonated because the recently reported hydrogenation catalytically active Mn-[hydrogenase], which has similar structural features as compound **1**, is activated in a similar way.[26] The deprotonation reaction was carried under a N_2 atmosphere at room temperature starting with $[Mn(CO)_3]_2(H_2ema)$ dissolved in THF with 2 equiv. of sodium hydride (NaH) to give complex **1** after less than 1 hour (Figure 10). The simple workup of **1** included a filtration through Celite® and cotton wool, following with evacuating the solvent and washing with pentane.

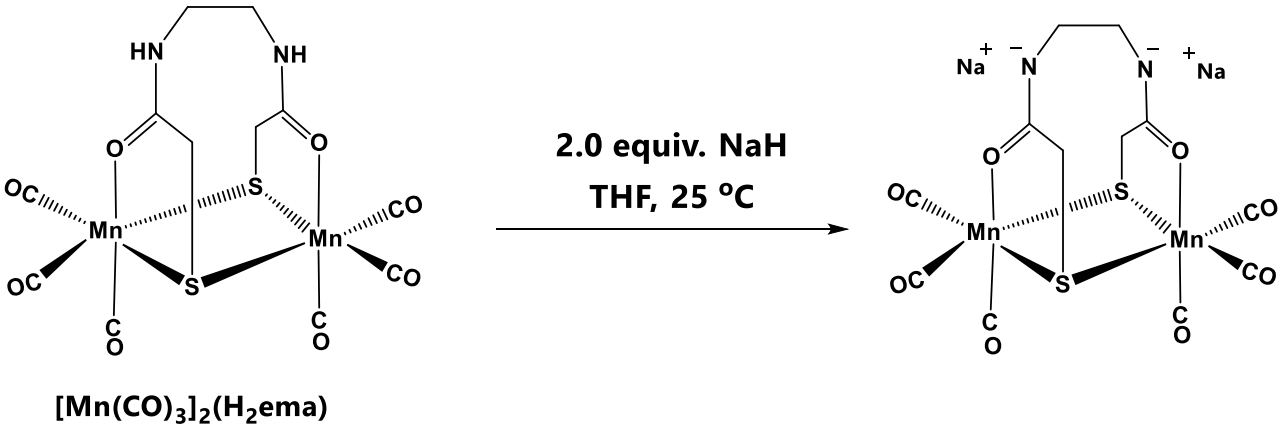

Figure 10. Deprotonation reaction of compound **1**

The completion of the reaction was monitored by infrared spectroscopy which showed a gradual shift of all signals (Figure 11 left). The infrared spectrum of the deprotonated **1** in THF exhibits five peaks at 1845, 1886, 1908, 1973, and 2008 cm^{-1}. All three ν(CO) signals from the starting material–complex **1**: 2025, 2005 and 1915 cm^{-1} significantly shifted to the lower frequency indicating that the two Mn centers become more electron-rich after the removal of the two protons. It should be noted that after the deprotonation, the broad signal at 1915 cm^{-1} in complex **1** shifted and separated into two signals, while the small shoulder signal at 1880 cm^{-1} ν from **1** became a clear signal at 1845 cm^{-1}. Assignments of both IR signals are necessary to understand the role of these hydrogens to the complex. Also, the same deprotonation reaction was carried simultaneously using NaOMe as a base instead of NaH to see basicity effect. The formation of the deprotonated **1** in this reaction was as steady as in the reaction using NaH and did not show any difference in IR spectra. This indicates that the base strength does not play a substantial role in this reaction. Compound **1** will be isolated and crystalized to look at the differences in bond lengths and angles, stability, and reactivities. The result rom this experiment is a success to the hydrogenation catalysis project; future studies will focus on applying appropriate substrates to test the activity of **1**.

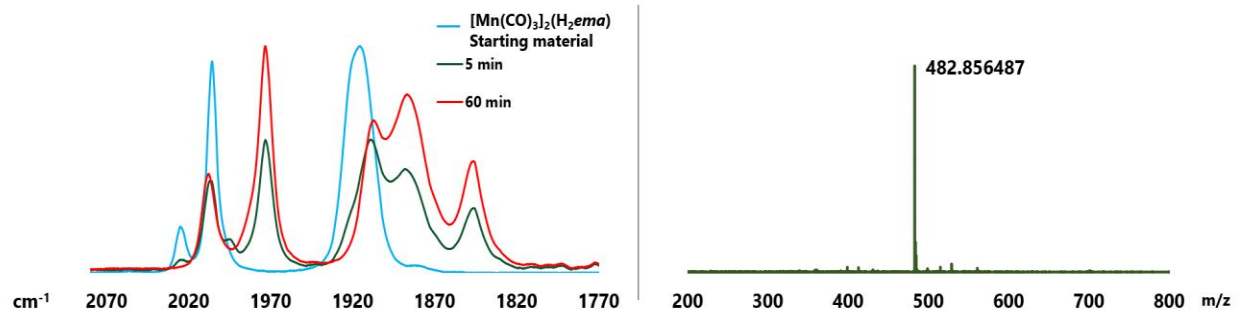

Figure 11. FR-IR spectra to monitor the deprotonation of **1** (left) and ESI-HRMS negative mode spectrum of **1** after 60 min of reaction

CHAPTER V

STRUCTURES OF Mn COMPLEXES INSPIRED BY $[Mn_2(CO)_3]_2(H_2ema)$

Mn_4S_4 carbonyl cluster

The works by the Nicholson group[25,27] motivated us to study more about hybrid hard/soft (O,S) chelating ligands in Mn complexes. Instead of using thiosalicylic acid[27] or thioglycolic acid[25] as in Nicholson's works, we react $Mn(CO)_5Br$ with methyl thioglycolate to make a structure that is more similar to compound **1**. The reaction at room temperature occurred readily in the presence of Et_3N. The reaction was monitored by IR spectroscopy in DCM (Figure 12). In a period of 4 h, the some signals of the starting material ($Mn(CO)_5Br$ diminish smoothly and new peaks appeared resulting in the total of 5 signals (green: 1734, 1905, 1990, 2005, 2050 cm^{-1}).

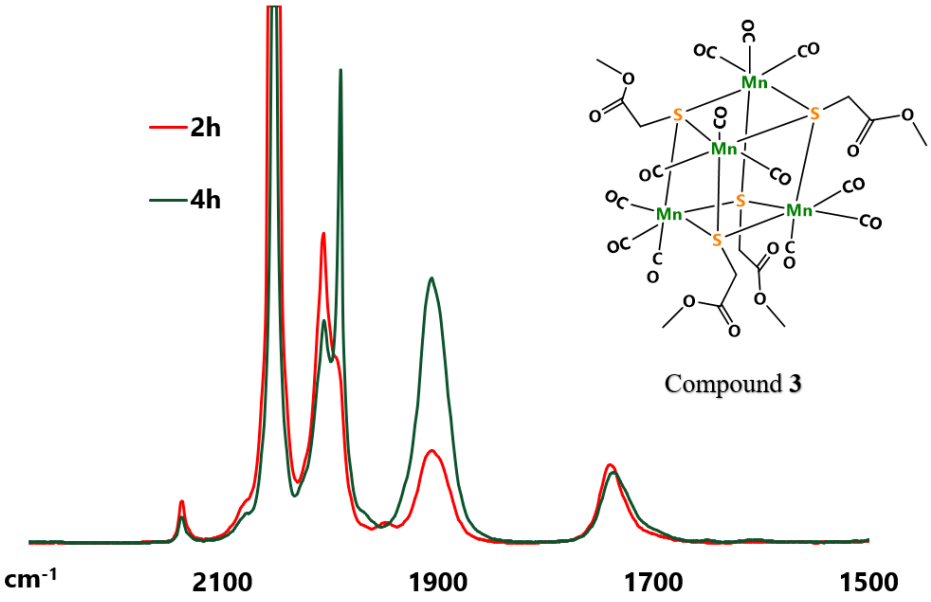

Figure 12. FT-IR spectra to monitor the synthesis of compound **3** in THF

Interestingly, crystallographic study for **3** elucidated a Mn_4S_4 cluster with thiolate ligands and 3 carbonyl ligands on each Mn centers (Figure 13). This cluster has a distorted cubic structure, in which the ∠S-Mn-C(O) angles range from 169 – 172^o. It was surprising that methyl thioglycolate did not become an S, O-donor ligand to Mn as seen in compound **1**, and in thioglycolate and thiosalicylato derivatives of Mn carbonyl.[25, 27] Other crystallographic data are included in Table 5 and crystal packing is shown in Figure 14.

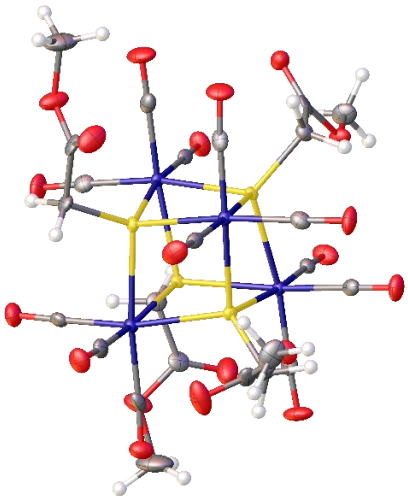

Figure 13. Crystal structure of complex 3

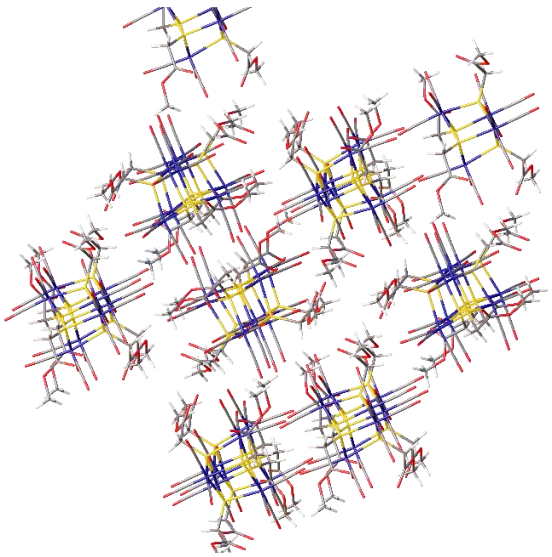

Figure 14. Packing diagram of **2**

Table 5. Crystal data and structure refinement for **3**

Empirical formula	$C_{12}H_{10}Mn_2O_{10}S_2$
Formula weight	488.20
Temperature/K	110
Crystal system	orthorhombic
Space group	$P2_12_12_1$
a/Å	10.3153(7)
b/Å	18.1610(12)
c/Å	18.7537(12)
α/°	90
β/°	90
γ/°	90
Volume/Å^3	3513.2(4)
Z	8
ρ_{calc}g/cm^3	1.846
μ/mm^{-1}	1.724
F(000)	1952.0
Crystal size/mm^3	0.1 × 0.1 × 0.1
Radiation	MoKα (λ = 0.71073)
2Θ range for data collection/°	3.122 to 61.098
Index ranges	$-14 \leq h \leq 14$, $-25 \leq k \leq 25$, $-26 \leq l \leq 26$
Reflections collected	66081
Independent reflections	10750 [R_{int} = 0.1070, R_{sigma} = 0.0932]
Data/restraints/parameters	10750/0/473
Goodness-of-fit on F^2	1.033
Final R indexes [I>=2σ (I)]	R_1 = 0.0507, wR_2 = 0.0698
Final R indexes [all data]	R_1 = 0.0827, wR_2 = 0.0767
Largest diff. peak/hole / e Å^{-3}	0.54/-0.57
Flack parameter	0.007(7)

Mn carbonyl complex bearing "half *ema*" ligand

As mentioned in the X-ray crystallographic study of **1**, manganese complexes where the five-membered rings are in the *anti*-position have been reported.[25] We ask whether an isomeric of **1**, where the two nitrogen atoms are not connected giving rise to the *anti*-position of two five-membered rings, can be obtained. First, N-(mercaptomethyl)acetamide generated from the reaction of $MeNH_2$ with methyl mercaptoacetate was brought to react with $Mn(CO)_5Br$ and Et_3N at room temperature to give complex **4** (Figure 15).

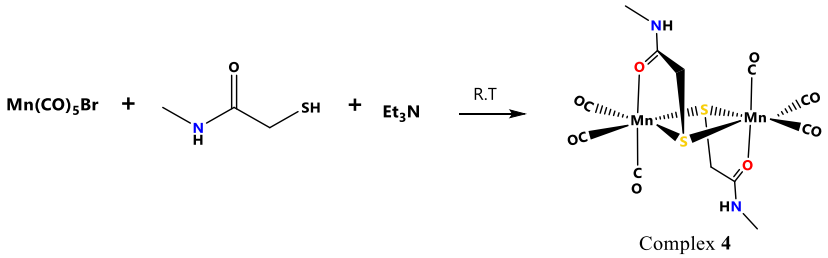

Figure 15. Synthesis of complex **4**

The IR spectra (Figure 16 left) used to monitor the reaction showed a gradual change in pattern from the starting material to **4**. The IR spectrum after 4 days of reacting showed three secondary amide signals below 1800 cm^{-1} and three carbonyl peaks at 2010, 2050, 2079 cm^{-1}. These IR peaks are similar to those of the thioglycolate manganese carbonyl reported by Nicholson[25] although shifted slightly to higher frequencies. IR signals also suggest that the CO chemical environments were changed compared with the original complex **1**. The ^{1}H-NMR of **4** (Figure 16 right) was also taken in $CDCl_3$ and showed a broad peak at 6.66 ppm is characteristic for the protons at the amido nitrogens.

X-ray quality crystals of **4** were obtained from vapor diffusion of pentane into the THF. Complex **4** crystalized in a mono clinic system and with a $P2_1/c$ space group. The crystal structure (Figure 17) elucidates the expected two sulfur-bridging ligands with two five-membered rings in

the *anti*-positions. The distance between two Mn centers is 3.586 Å, which is approximately the same as in complex **1** (3.566 Å) and Nicholson's thioglycolate manganese carbonyl (3.567 Å). Interestingly, the 'bite' angle ∠S-Mn-O of complex **4** (82.7°) is very close to the one of Nicholson's complex (82.3°), which is smaller than the bite angle in complex **1** (93.6°). Other crystallographic data are included in table 6 and 7 and the packing diagram is shown in Figure 18.

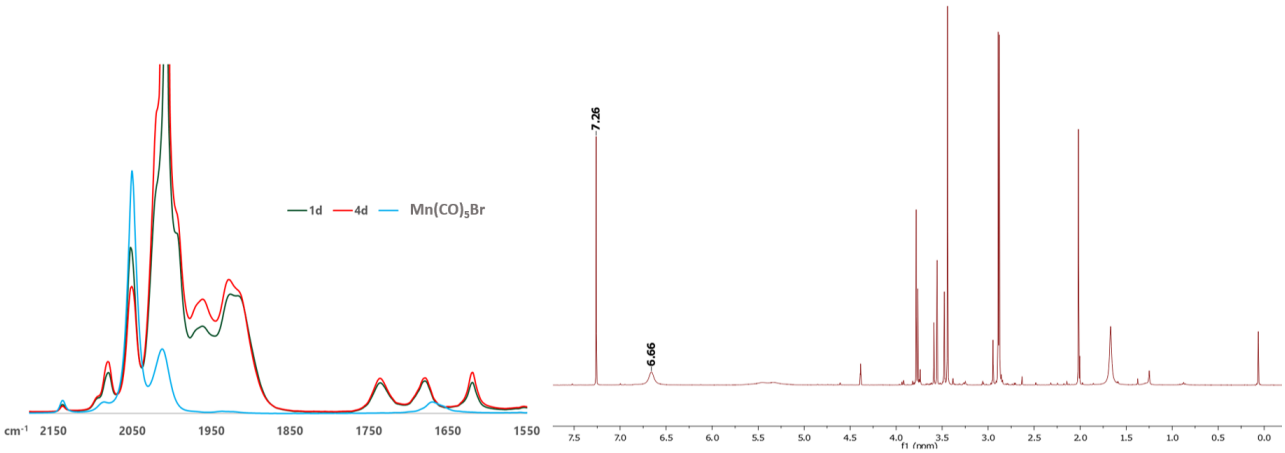

Figure 16. FT-IR and ^{1}H-NMR spectra of **4**

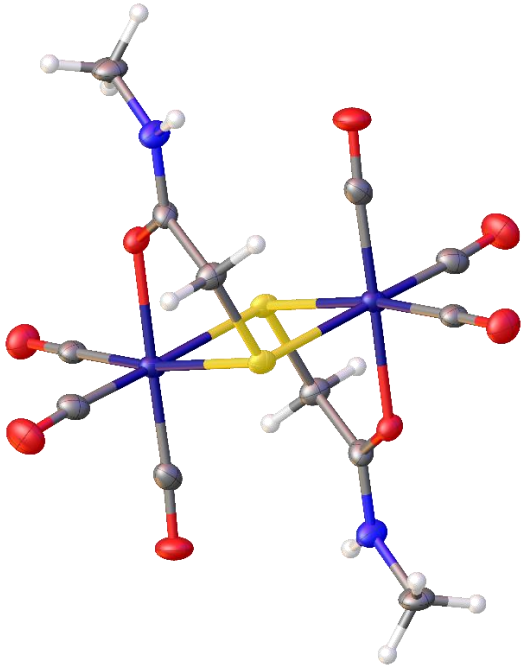

Figure 17. Crystal structure of complex **4**

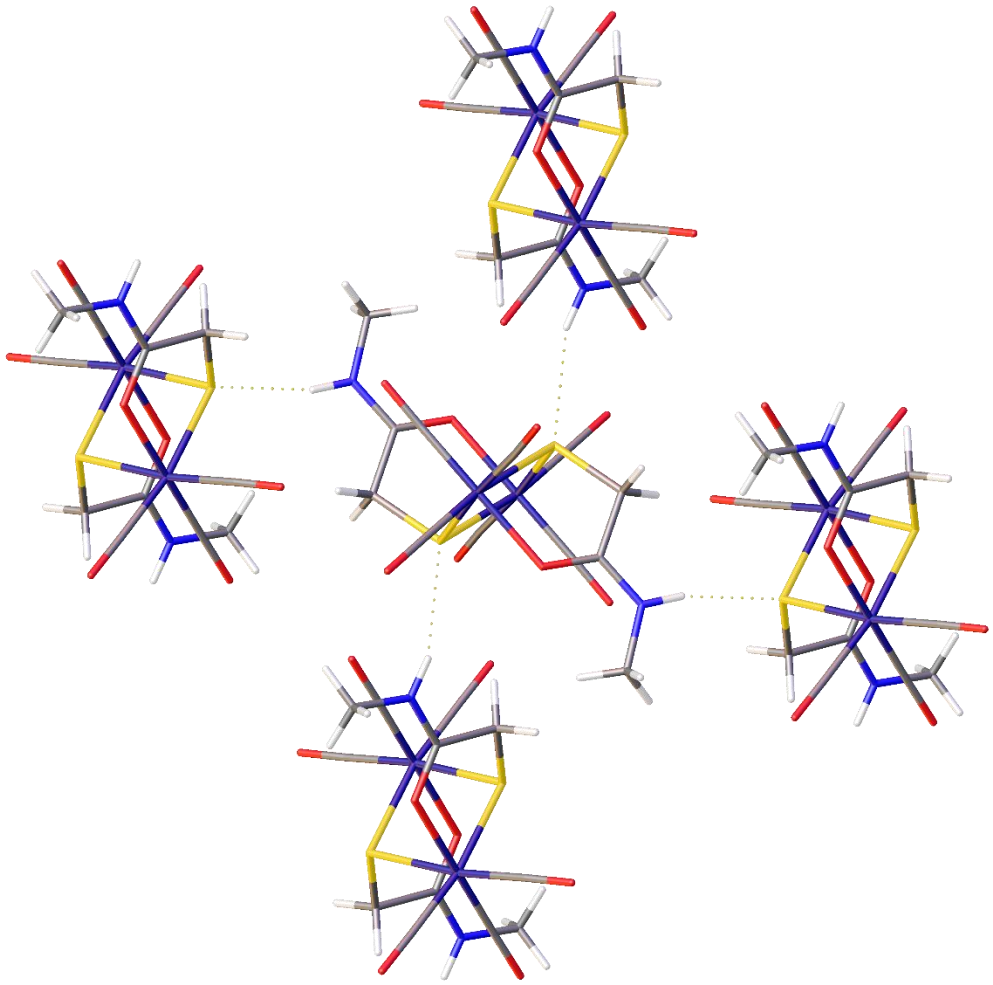

Figure 18. Packing diagram of **4** with dotted lines represent H-bonds

Table 5. Selected bond lengths in complex **4**

Atom	Atom	Length/Å		Atom	Atom	Length/Å
Mn01	S002[1]	2.3878(11)		O003	C008	1.257(4)
Mn01	S002	2.3744(11)		O004	C00C	1.151(4)
Mn01	O003	2.055(3)		O005	C009	1.156(5)
Mn01	C009	1.791(4)		O006	C00A	1.147(5)
Mn01	C00A	1.810(4)		N007	C008	1.316(5)
Mn01	C00C	1.813(4)		N007	C00D	1.460(5)
S002	C00B	1.820(4)		C008	C00B	1.507(5)

Table 6. Crystal data and structure refinement for **4**

Empirical formula	$C_{12}H_{12}Mn_2N_2O_8S_2$
Formula weight	486.24
Temperature/K	110
Crystal system	monoclinic
Space group	$P2_1/c$
a/Å	8.1440(7)
b/Å	10.6160(9)
c/Å	10.4277(9)
α/°	90
β/°	97.903(2)
γ/°	90
Volume/Å^3	892.98(13)
Z	2
ρ_{calc}g/cm^3	1.808
μ/mm^{-1}	1.691
F(000)	488.0
Crystal size/mm^3	0.2 × 0.1 × 0.1
Radiation	MoKα (λ = 0.71073)
2Θ range for data collection/°	5.05 to 60.614
Index ranges	$-11 \leq h \leq 11$, $-15 \leq k \leq 15$, $-14 \leq l \leq 14$
Reflections collected	57630
Independent reflections	2670 [R_{int} = 0.1556, R_{sigma} = 0.0677]
Data/restraints/parameters	2670/0/119
Goodness-of-fit on F^2	1.139
Final R indexes [I>=2σ (I)]	R_1 = 0.0645, wR_2 = 0.1007
Final R indexes [all data]	R_1 = 0.1022, wR_2 = 0.1087
Largest diff. peak/hole / e Å^{-3}	0.66/-0.80

CHAPTER VI

CONCLUSION

When choosing $M(ema)^{2-}$ as the MN_2S_2 ligand to react with $Mn(CO)_5Br$, an unprecedented result was obtained, in which M is removed from the tetradentate tight binding site and '*ema*' becomes a tridentate binucleating S_2O_2 ligand to a two-manganese bimetallic system. Characterizations of this novel compound $[Mn(CO)_3]_2(H_2ema)$ were achieved by using infrared spectroscopy, X-Ray diffraction, nuclear magnetic resonance spectroscopy, and mass spectrometry. Different synthetic approaches to $[Mn(CO)_3]_2(H_2ema)$ with modified starting materials reveal a fascinating metal-templated process where folding the backbone of ema ligand is essential to target the final product. This folding process is also reminiscent of tight loops in proteins. The solid-state structure of $[Mn(CO)_3]_2(H_2ema)$ determined via X-ray diffraction shows a pseudo-octahedral geometry around each manganese center which has two bridging thiolate sulfurs, three carbonyls, and one carboxamide oxygen. In addition, two five-membered Mn-S-CH_2-C-O rings in which manganese centers reside both hard and soft ligand donor sites suggest prospective applications and exciting reactivities of this complex.

Related studies of this novel complex including the synthesis of the Re analogue and the reactivity experiments were done. $^{13}CO/^{12}CO$ exchange experiments proved the different in chemical environments of the CO ligands. $[Mn(CO)_3]_2(H_2ema)$ showed the ability to be deprotonated in a presence of a base suggesting the potential catalytic activity. Future studies for $[Mn(CO)_3]_2(H_2ema)$ will center around its catalytic ability and its structural features including the bond hemilability.

To investigate the hybrid hard/soft (O,S) chelating ligands in Mn complexes, two new complexes are synthesized from reaction of $Mn(CO)_5Br$ with methyl thioglycolate and N-(mercaptomethyl)acetamide. The prior reaction yield an interesting Mn_4S_4 carbonyl cluster, while the latter one resulted in a isomeric of $[Mn(CO)_3]_2(H_2ema)$, where the two identical 'half *ema*' bidentate ligands bind to two Mn centers to enable *anti*-positions for the two five-membered rings. X-ray quality crystals of both complexes were successfully isolated to support the spectroscopic data. The next step of this project is to study the reactivities of these two complexes and compare them to $[Mn(CO)_3]_2(H_2ema)$.

In general, the library of N_2S_2 ligands has not been totally explored and understood and there are many metals that have not been applied to these gorgeous ligands. The mathematical combination of these two components, ligand and metal, yields a uncountably big number; therefore, there are always rooms for new breakthroughs in this area. The novelty of this work is hoped to one way or another contribute to the current extensive developments of biomimetic chemistry, catalysis, organometallics, and sustainable chemistry.

REFERENCES

(1) Kovacs, J. A. Synthetic analogues of cysteinate-ligated non-heme iron and non-corrinoid cobalt enzymes. *Chem. Rev.* **2004**, *104*, 825-848.

(2) Huang, W. J.; Jia, J.; Cummings, J.; Nelson, M.; Schneider, G.; Lindqvist, Y. Crystal structure of nitrile hydratase reveals a novel iron centre in a novel fold. *Structure* **1997**, *5*, 691-699.

(3) Green, K. N.; Brothers, S. M.; Lee, B.; Darensbourg, M. Y.; Rockcliffe, D. A. Chemical Issues Addressing the Construction of the Distal Ni Cysteine-Glycine-Cysteine (2-) Site of Acetyl CoA Synthase: Why Not Copper? *Inorg. Chem.* **2009**, *48*, 2780-2792.

(4) Doukov, T. I.; Iverson, T. M.; Seravalli, J.; Ragsdale, S. W.; Drennan, C. L. A Ni-Fe-Cu center in a bifunctional carbon monoxide dehydrogenase/acetyl-CoA synthase. *Science* **2002**, *298*, 567-572.

(5) Denny, J. A.; Darensbourg, M. Y. Metallodithiolates as Ligands in Coordination, Bioinorganic, and Organometallic Chemistry. *Chem. Rev.* **2015**, *115*, 5248-5273.

(6) Denny, J. A.; Foley, W. S.; Todd, A. D.; Darensbourg, M. Y. The ligand unwrapping/rewrapping pathway that exchanges metals in S-acetylated, hexacoordinate $N_2S_2O_2$ complexes. *Chem. Sci.* **2015**, *6*, 7079-7088.

(7) Jenkins, R. M.; Pinder, T. A.; Hatley, M. L.; Reibenspies, J. H.; Darensbourg, M. Y. Tetradentate N_2S_2 Vanadyl(IV) Coordination Complexes: Synthesis, Characterization, and Reactivity Studies. *Inorg. Chem.* **2011**, *50*, 1849-1855.

(8) Rampersad, M. V.; Jeffery, S. P.; Golden, M. L.; Lee, J.; Reibenspies, J. H.; Darensbourg, D. J.; Darensbourg, M. Y. Characterization of steric and electronic properties of NiN_2S_2 complexes as S-donor metallodithiolate ligands. *J. Am. Chem. Soc.* **2005**, *127*, 17323-17334.

(9) Lunsford, A. M.; Goldstein, K. F.; Cohan, M. A.; Denny, J. A.; Bhuvanesh, N.; Ding, S. D.; Hall, M. B.; Darensbourg, M. Y. Comparisons of MN2S2 vs. bipyridine as redox-active ligands to manganese and rhenium in (L-L)M'$(CO)_3$Cl complexes. *Dalton Trans.* **2017**, *46*, 5175-5182.

(10) Hawecker, J.; Lehn, J. M.; Ziessel, R. Efficient Photochemical Reduction of CO2 to CO by Visible-Light Irradiation of Systems Containing $Re(Bipy)(CO)_3X$ or $Ru(Bipy)_3^{2+}$ - CO_2^+ Combinations as Homogeneous Catalysts. *J. Chem. Soc., Chem. Commun.* **1983**, 536-538.

(11) Smieja, J. M.; Kubiak, C. P. $Re(bipy\text{-}tBu)(CO)_3Cl$-improved Catalytic Activity for Reduction of Carbon Dioxide: IR-Spectroelectrochemical and Mechanistic Studies. *Inorg. Chem.* **2010**, *49*, 9283-9289.

(12) Benson, E. E.; Kubiak, C. P.; Sathrum, A. J.; Smieja, J. M. Electrocatalytic and homogeneous approaches to conversion of CO_2 to liquid fuels. *Chem. Soc. Rev.* **2009**, *38*, 89-99.

(13) Bourrez, M.; Molton, F.; Chardon-Noblat, S.; Deronzier, A. $Mn(bipyridyl)(CO)_3Br$: An Abundant Metal Carbonyl Complex as Efficient Electrocatalyst for CO2 Reduction. *Angew. Chem. Int. Ed.* **2011**, *50*, 9903-9906.

(14) Grills, D. C.; Farrington, J. A.; Layne, B. H.; Lymar, S. V.; Mello, B. A.; Preses, J. M.; Wishart, J. F. Mechanism of the Formation of a Mn-Based CO_2 Reduction Catalyst Revealed by Pulse Radiolysis with Time-Resolved Infrared Detection. *J. Am. Chem. Soc.* **2014**, *136*, 5563-5566.

(15) Ngo, K. T.; McKinnon, M.; Mahanti, B.; Narayanan, R.; Grills, D. C.; Ertem, M. Z.; Rochford, J. Turning on the Protonation-First Pathway for Electrocatalytic CO_2 Reduction by Manganese Bipyridyl Tricarbonyl Complexes. *J. Am. Chem. Soc.* **2017**, *139*, 2604-2618.

(16) Agarwal, J.; Shaw, T. W.; Schaefer, H. F.; Bocarsly, A. B. Design of a Catalytic Active Site for Electrochemical CO_2 Reduction with Mn(I)-Tricarbonyl Species. *Inorg. Chem.* **2015**, *54*, 5285-5294.

(17) Costentin, C.; Drouet, S.; Robert, M.; Saveant, J. M. A Local Proton Source Enhances CO_2 Electroreduction to CO by a Molecular Fe Catalyst. *Science* **2012**, *338*, 90-94.

(18) Sung, S.; Li, X. H.; Wolf, L. M.; Meeder, J. R.; Bhuvanesh, N. S.; Grice, K. A.; Panetier, J. A.; Nippe, M. Synergistic Effects of Imidazolium-Functionalization on fac-$Mn(CO)_3$ Bipyridine Catalyst Platforms for Electrocatalytic Carbon Dioxide Reduction. *J. Am. Chem. Soc.* **2019**, *141*, 6569-6582.

(19) Sampson, M. D.; Nguyen, A. D.; Grice, K. A.; Moore, C. E.; Rheingold, A. L.; Kubiak, C. P. Manganese Catalysts with Bulky Bipyridine Ligands for the Electrocatalytic Reduction of Carbon Dioxide: Eliminating Dimerization and Altering Catalysis (vol 136, pg 5460, 2014). *J. Am. Chem. Soc.* **2015**, *137*, 3718-3718.

(20) Kruger, H. J.; Peng, G.; Holm, R. H. Low-Potential Nickel(III, II) Cpmplexes - New Systems Based On Tetradentate Amidate Thiolate Ligands and the Influence of Ligand Structure on Potentials in Relation to the Nickel Site in NiFe- Hydrogenases. *Inorg. Chem.* **1991**, *30*, 734-742.

(21) Mull, E. S.; Sattigeri, V. J.; Rodriguez, A. L.; Katzenellenbogen, J. A. Aryl cyclopentadienyl tricarbonyl rhenium complexes: Novel ligands for the estrogen receptor with potential use as estrogen radiopharmaceuticals. *Biorg. Med. Chem.* **2002**, *10*, 1381-1398.

(22) Jaouen, G.; Top, S.; Vessieres, A.; Pigeon, P.; Leclercq, G.; Laios, I. First anti-oestrogen in the cyclopentadienyl rhenium tricarbonyl series. Synthesis and study of antiproliferative effects. *Chem. Commun.* **2001**, 383-384.

(23) Bethel, R. D.; Crouthers, D. J.; Hsieh, C. H.; Denny, J. A.; Hall, M. B.; Darensbourg, M. Y. Regioselectivity in Ligand Substitution Reactions on Diiron Complexes Governed by Nucleophilic and Electrophilic Ligand Properties. *Inorg. Chem.* **2015**, *54*, 3523-3535.

(24) Le, T.; Nguyen, H.; Perez, L. M.; Darensbourg, D. J.; Darensbourg, M. Y. Metal-Templated, Tight Loop Conformation of a Cys-X-Cys Biomimetic Assembles a Dimanganese Complex. *Angew. Chem. Int. Ed.* **2020,** *59*, 3645-3649.

(25) Dai, Y.; Nicholson, B. K. Synthesis and Structure of a Dimeric, Anionic Thioglycolate Derivative of Man-ganese Carbonyl. *Aust. J. Chem.* **2012,** 65, 730–73.

(26) Pan, H. J.; Huang, G. F.; Wodrich, M. D.; Tirani, F. F.; Ataka, K.; Shima, S.; Hu, X. L. A catalytically active Mn -hydrogenase incorporating a non-native metal cofactor. *Nat. Chem.* **2019**, *11*, 669-675.

(27) Depree, C.; Main, L.; Nicholson, B. K.; Roberts, K. Preparation and structures of tetrameric and dimeric manganese carbonyl complexes incorporating thiosalicylato ligands, *J. Organomet. Chem.* **1996,** *517*, 201-207.